Short Communication

Solid octahedral NiO micro-particles prepared by a calcination method in the presence of an ionic liquid and their application as anode for lithium ion batteries

Xuan Zhang[1], Keqiang Ding[1, 2,*], Xiaojing Gao[2], Xiaomi Shi[2], Jingwei Han[2], Junqing Pan[1,*]

[1] State Key Laboratory of Chemical Resource Engineering, Beijing University of Chemical Technology, Beijing, 100029, P.R.China
[2] College of Chemistry and Materials Science, Hebei Normal University, Shijiazhuang 050024, P.R. China
*E-mail: dkeqiang@263.net (K. Ding.); jqpan@mail.buct.edu.cn (J. Pan)

A novel finding, that solid octahedral NiO micro-particles can be prepared via an ionic liquid (IL)-present calcination method using nickel acetate as the starting material, was reported for the first time in this communication. In the absence of IL, NiO particles with a porous cauliflower-like morphology were produced. The crystal structure and the morphologies of all synthesized samples were respectively characterized by using X-ray diffraction (XRD) and scanning electron microscopy (SEM). The formation of NiO phase in sample a was further verified via HRTEM and XPS. Also, it was revealed by the galvanostatic charge-discharge measurement that the initial discharge capacity of the solid octahedral NiO micro-particles was 757.3 mAh g^{-1} at 100 mA g^{-1}, much larger than that of sample b (436.3 mAh g^{-1}). And even after 50 cycles, the discharge capacities of all prepared samples were all maintained higher than 210 mAh g^{-1} at 100 mA g^{-1}. The successful preparation of solid octahedral NiO micro-particles was very favorable not only for the development of lithium ions anode materials but also for the exploration of micro-scale devices.

1. INTRODUCTION

Recently, several typical transition metal oxides have been successfully explored as anode materials for LIBs with an intention to replace the current commercial anode material of graphite. Among these transition metal oxides anode materials, NiO was also demonstrated to be a promising anode material for LIBs mainly due to its relatively higher theoretical capacity (718 mAh g^{-1}), low cost and environmental friendliness [1]. However, recent research works concerning NiO revealed that the

large volume variation during the cycling process and the lower electrical conductivity were the main two obstacles for the real life applications of NiO as anode material for LIBs [2]. Thus, many strategies have been proposed to promote the electrochemical performance of NiO in recent years. In general speaking, creating nano-sized NiO particles [3] and being composited with carbon [4] were regarded as the major two approaches to solve above two issues. Except for above two conventional approaches, preparing NiO particles with special morphology is also a feasible way to enhance the electrochemical behavior of NiO anode material since the electrochemical property of an anode material is also closely related to its morphology. Thus far, NiO particles with various morphologies like hollow microsphere, egg shell-yolk nanostructure, porous nanobelt and nanosheet have been successfully created to meet the demand of employing NiO in various research fields (such as photocatalysis, ultraviolet sensors, magnetic material, water treatment material). However, to the best of our knowledge, the synthesis of solid octahedral NiO micro-particles via an IL-present calcination method has not yet been reported though the preparation of solid octahedral NiO particles and hollow octahedral NiO particles has been, respectively, addressed by Jin [5] and Yuan's research group [6]. In Jin's work [5], $NiCl_2 \cdot 6H_2O$ and NaOH were used as the starting materials, and the size of all prepared solid octahedral NiO particles was less than 0.15 μm. In Yuan's work [6], the starting materials were $NiCl_2 \cdot 6H_2O$ and carbon spheres, being rather different from our works described here.

In this work, a very facile IL-present calcination method was developed, and solid octahedral NiO micro-particles were successfully prepared.

2. EXPERIMENTAL SECTION

Firstly, a proper amount of nickel acetate and 0.5 g IL of 1-butyl-3-methylimidazolium chloride salt were thoroughly dissolved in 10 mL redistilled water, and then 10 mL anhydrous ethanol was added into above solution drop by drop carefully. Afterwards, the resultant solution was vigorously stirred for 30 min at room temperature. Subsequently, the resultant solution was placed in a capped crucible which was heated in a muffle furnace at 600 °C for 2 h. The samples produced with IL and without IL were respectively nominated as sample a and b.

3. RESULTS AND DISCUSSION

The XRD patterns of the as-synthesized samples are illustrated in Fig.1(a). For sample a, the diffraction peaks positioned at around 37.4º, 43.5º, 63.1º and 75.7º matched well with the crystal facets of (110), (200), (220) and (311) of NiO (JCPDS no.00-047-1049) [7], confirming the formation of NiO phase in sample a. While, for sample b, besides above diffraction peaks, two peaks appearing at 44.6º and 52.0º could be respectively indexed to the lattice plane of (111) and (200), which effectively indicated that a proper amount of pure metallic Ni phase was produced in sample b through comparing with the standard pattern of metallic Ni (JCPDS, no.01-087-0712).

SEM images for the prepared samples are displayed in Fig.1(b). Many solid octahedral NiO

micro-particles are distinctly observed in sample a. The size of these solid octahedral particles ranged from 0.4 μm to 1 μm, being significantly larger than that of the nano octahedral NiO particles prepared by Jin's group [5]. While, in the case of sample b (image b of Fig.1(b)), many porous cauliflower-like large particles with a hierarchical morphology are exhibited clearly. The patterns of the EDS analysis for the synthesized samples are given in Fig.1(c). The peaks corresponding to C, O and Ni elements are clearly displayed. Therefore, it can be concluded that both sample a and b were a composite rather than a pure substance.
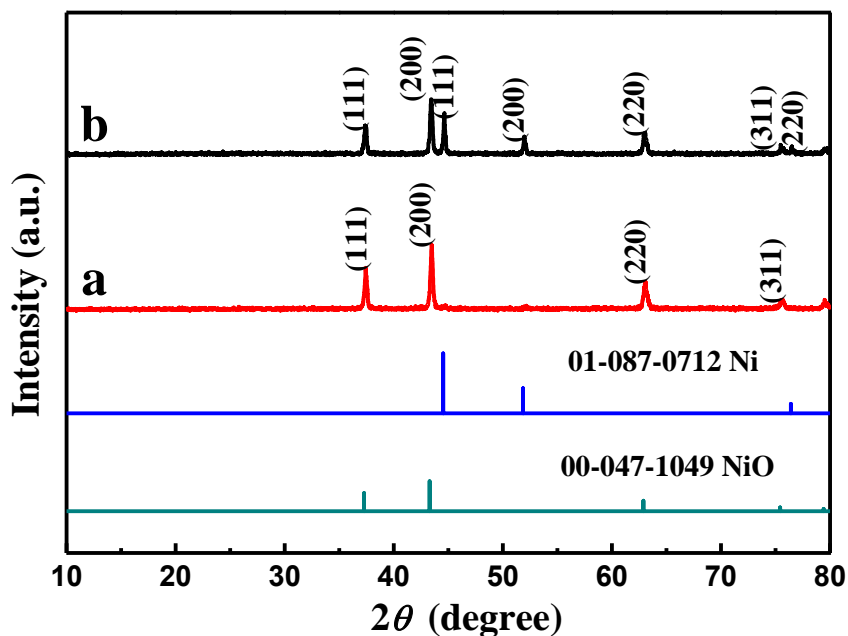
Figure 1(a). XRD patterns for sample a and b as well as the standard pattern of NiO and Ni. Pattern a and b corresponded to sample a and b.
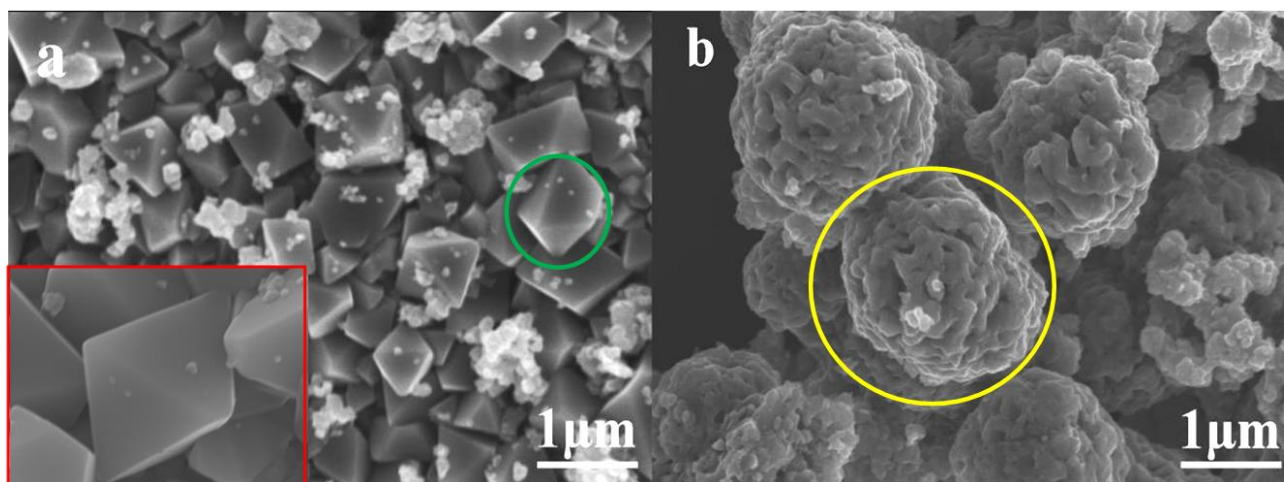
Figure 1(b). SEM images of the as-prepared samples. Image a and b corresponded to sample a and b. The image in the lower-left corner was the magnified image of sample a.
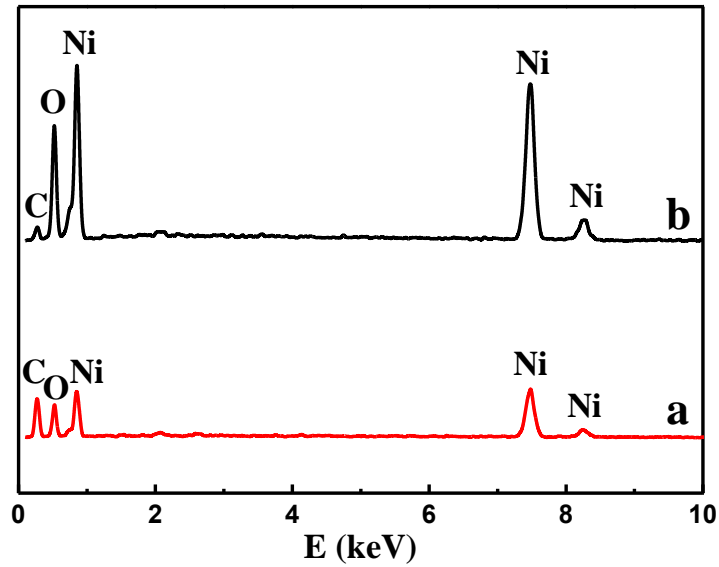
Figure 1(c). EDS spectra for all synthesized samples. Curve a and b correspond to sample a and b.
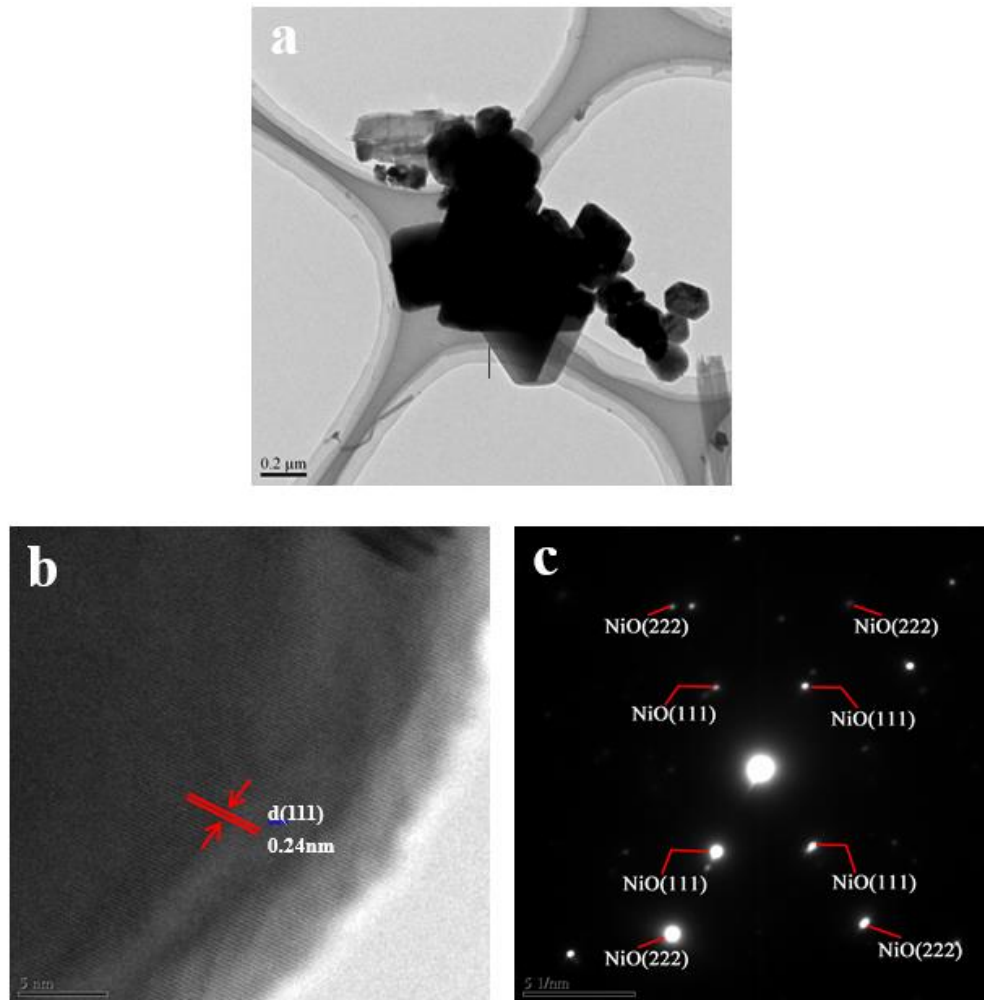
Figure 1(d). (a) TEM image for sample a; (b) The crystal lattice fringes in the HRTEM images of sample a ; (c) SAED patterns for sample a.

The solid octahedral NiO micro-particles were further characterized by HRTEM, and the results are illustrated in Fig.1(d). As seen from the image a of Fig.1(d), some smaller particles with well-defined cubic crystal structure are clearly exhibited, which effectively indicated that the solid octahedral NiO micro-particles shown in Fig.1(b) were constructed by many smaller cubic NiO crystal particles. The inter-planar distance for the (111) crystal face of sample a, as seen from the image b of Fig.1(d), was found to be 0.24 nm, which agreed well with the previous report concerning pristine NiO [3]. The presence of bright NiO (222) and (111) diffraction spots in the selected area electron diffraction (SAED) patterns (image c of Fig.1(d)) effectively indicated that solid octahedral NiO particles not only had an obvious crystallization but also had a polycrystalline nature [8].

As shown in the wide XPS survey spectra of Fig.2(a), the sharp peaks positioned at 855.1, 532.7 and 287.5eV were indexed to the characteristic peak of Ni2p, O1s and C1s, respectively, revealing the existence of nickel, oxygen and carbon element in all prepared samples. In the C1s high-resolution spectrum (Fig.2(b)), the peaks located at 284.8 and 288.2 eV, respectively, corresponded to the presence of nonoxygen carbon likes C-C or C=C, and carbon in carboxyl groups (HO-C=O) in the prepared samples [9]. In the high-resolution O1s spectrum (Fig.2(c)), the peak at 529.6 eV could be assigned to the characteristic Ni-O bond, and the peak centered at 531.9eV was originated from the surface species like hydroxyls, under-coordinated lattice oxygen and chemisorbed oxygen [10]. In the case of Ni 2p XPS spectrum (Fig. 2(d)), the pair of peaks appearing in the 850-865 eV were attributed to the Ni 2p3/2 spin orbit levels of NiO, and the other pair of peaks emerging in 870-885 eV were from the Ni2p1/2 of NiO [9, 10]. Careful observation also indicated that a small peak at 852.5 eV appeared in pattern b of Fig.2(d), further confirming the existence of metallic Ni in sample b [10].
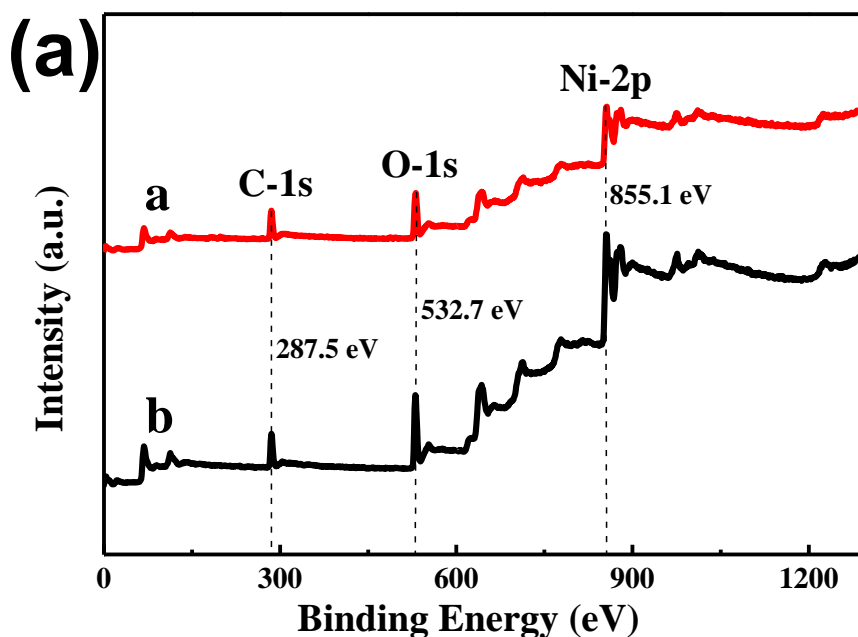
Figure 2(a). Wide scan XPS survey spectra for sample a (red curve) and b (black curve)

(b) C-1s

Intensity (a.u.)

284.8 eV

a

288.2 eV

b

Binding Energy (eV)
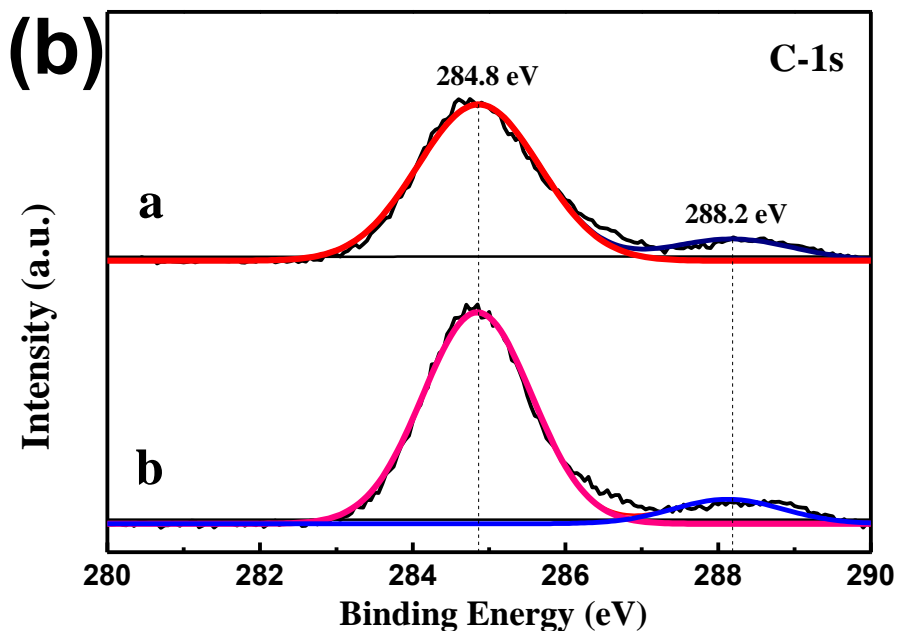
Figure 2(b). C1s spectrum of XPS spectra for prepared samples. Curve a and b corresponded to sample a and b.

(c) Ni-O   O-1s

Intensity (a.u.)

529.6 eV   531.9 eV

a

b

531.6 eV

Binding Energy (eV)
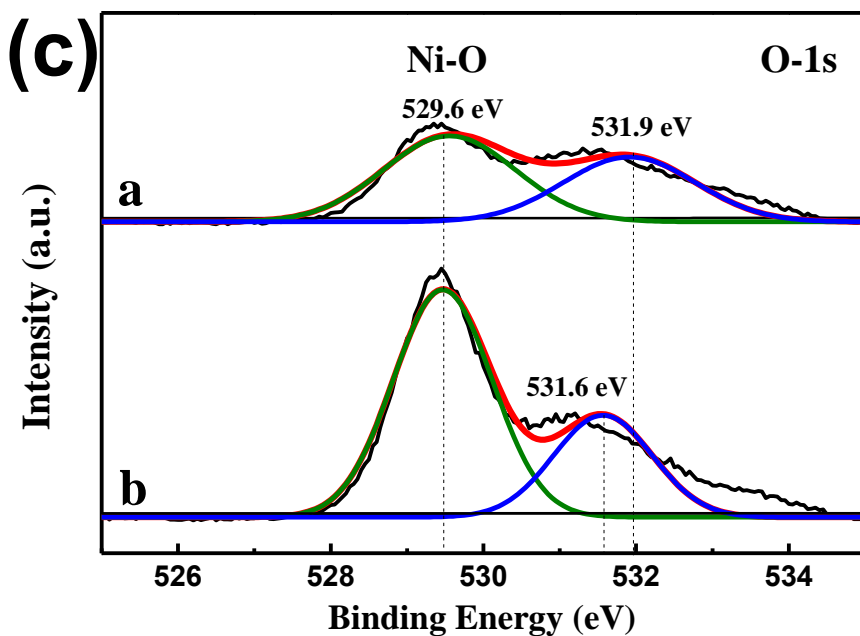
Figure 2(c). O1s spectrum of XPS spectra for prepared samples. Curve a and b corresponded to sample a and b.
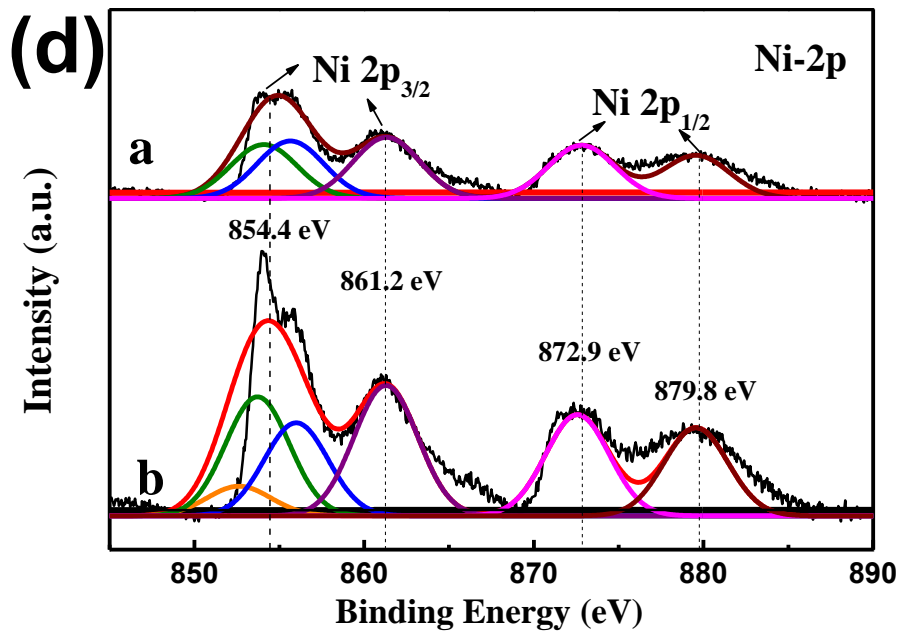
Figure 2(d). Ni2p spectrum of XPS spectra for prepared samples. Curve a and b corresponded to sample a and b.
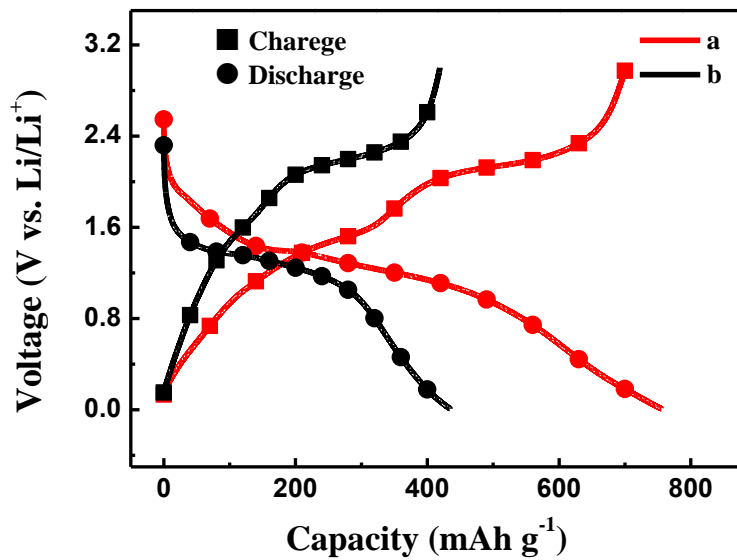
Figure 3(a). The initial charge-discharge profiles for sample a and b measured at 100 mA g^{-1} within the potential range of 0.01-3.0 V. Curve a and b corresponded to sample a and b.
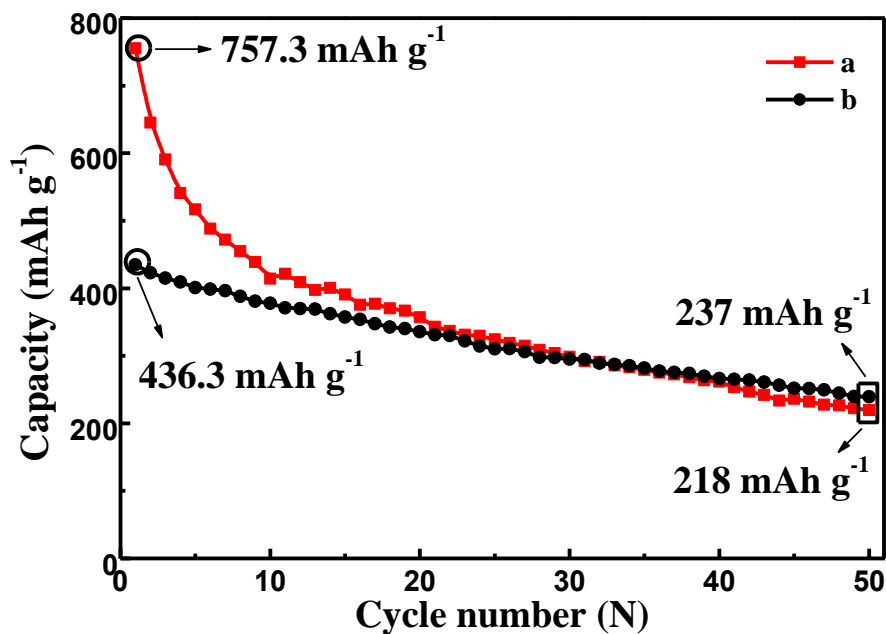
Figure 3(b).7. Cycling performance of two samples at a current density of 100 mA g⁻¹. Curve a and b corresponded to sample a and b.
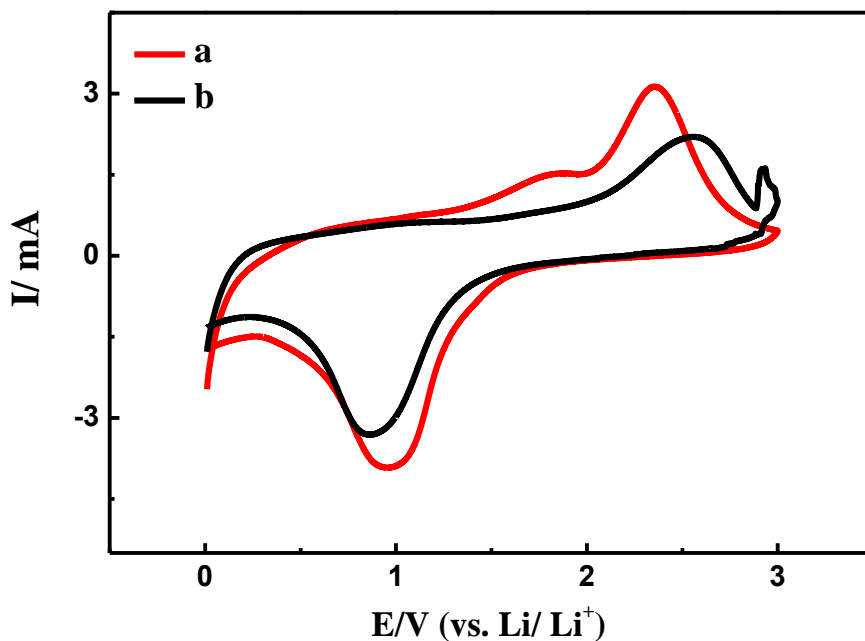
Figure 3(c). Cyclic voltammetry (CV) curves for sample a and b measured at the scan rate of 1mV s⁻¹. Curve a and b corresponded to sample a and b.
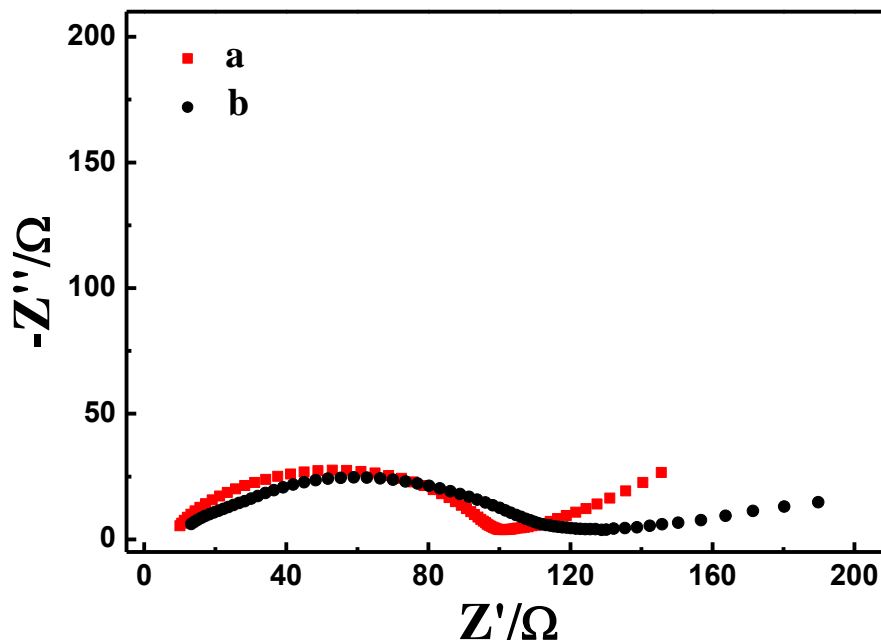
Figure 3(d). Nyquist plots obtained from EIS. Curve a and b corresponded to sample a and b.
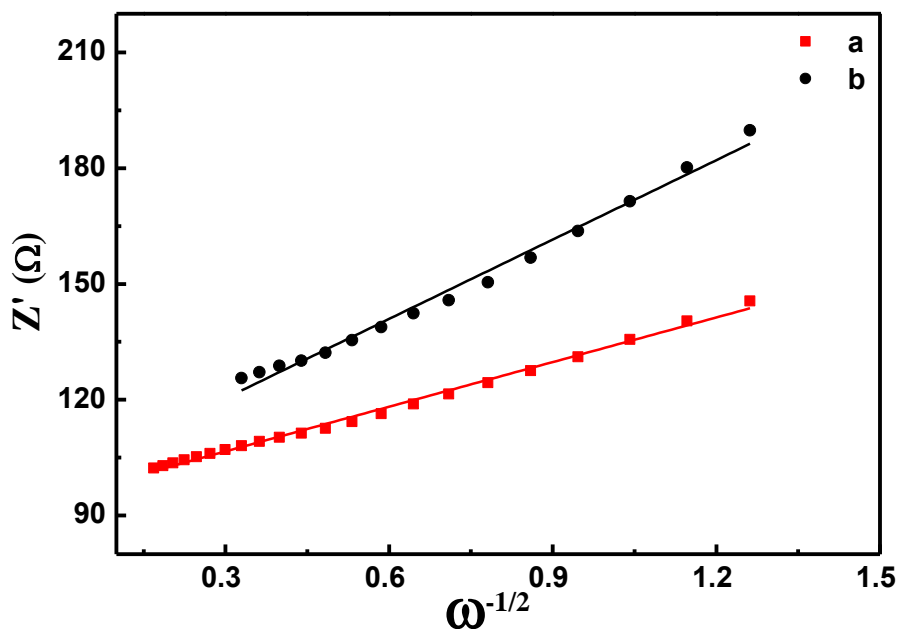
Figure 3(e). Curves describing the relationship between Z' and $\omega^{-1/2}$. Curve a (red rectangular box line) and b (black rectangular box line) corresponded to sample a and b.

Fig.3(a) shows the initial charge-discharge profiles of the as-prepared samples which was very similar to those of pristine NiO, further assuring that the main component of produced samples was NiO [11]. The initial discharge and charge capacities for sample a and b at 100 mA g^{-1} were measured to be 757.3 and 702 mAh g^{-1}, 436.3 and 420.4 mAh g^{-1}, respectively, showing a Coulombic efficiency of 92.6% and 96.4%. Noticeably, the discharge capacity value of 757.3 mAh g^{-1} of sample a was significantly larger than that of the NiO/C hollow microsphere (602 mAh g^{-1} at 100 mA g^{-1}) [7]. As shown in Fig.3(b), after 50 cycles, the discharge capacities of sample a and b at 100 mA g^{-1}

decreased gradually from 757.3 to 218 mAh g^{-1}, and from 435.8 to 237 mAh g^{-1}, respectively. Interestingly, the discharge capacities of 218 and 237 mAh g^{-1} were all remarkably larger than the theoretical capacity of lithium titanate (Li$_4$Ti$_5$O$_{12}$, 175 mAh g^{-1}) [12], suggesting that all the as-prepared samples could be employed as promising anode materials for LIBs.

The cyclic voltammetry (CV) curves of two prepared samples are plotted in Fig.3(c). For sample a, the peak potential separation ΔE_p ($\Delta E_p = E_{pa}-E_{pc}$) value was estimated to be 1.38 V, much smaller than that of sample b (1.70V). Generally, a smaller value of ΔE_p corresponded to a better reversibility of an electrode reaction [13]. Thus, within 20 cycles, sample a delivered a larger discharge capacity than sample b.

The Nyquist plots of all prepared samples are illustrated in Fig.3(d), from which the R$_{ct}$ values of sample a and b were evaluated to be 98 and 118 Ω, respectively. The diffusion efficiency of Li ions (D$_{Li}$) could also be estimated from the Nyquist plot using the following equation (1) and (2) [14,15].

$$D_{Li} = \frac{(RT)^2}{2(An^2F^2C_{Li}\sigma)^2} \tag{1}$$

$$Z_{re} = R_s + R_{ct} + \sigma\,\omega^{-1/2} \tag{2}$$

In equation (1), only σ was a novel parameter (Warburg factor) which could be acquired from the equation (2). In equation (2), Z$_{re}$ was the real part of the impedance, in our work, Z$_{re}$ was Z'. Thus, the value of σ was just the slope of the line describing the relationship of between Z$_{re}$ and $\omega^{-1/2}$. As shown in Fig.3(e), the σ value for sample a was much lower than that of sample b. It effectively indicated that a larger value of D$_{Li}$ was exhibited by sample a compered with sample b, when supposing that all other parameters in equation (1) for sample a were identical to those of sample b.

4. CONCLUSION

For the first time, an ionic liquid (IL)-present calcination method was developed for preparing solid octahedral NiO micro-particles. The successful preparation of solid octahedral NiO micro-particles was beneficial not only for the development of anode materials for LIBs but also for the exploration of micro-scale devices.

References

1. X. Ruan, Y. Yang, K. Pu, M. Gao, Y. Liu and H. Pan, *J. Power Sources,* 397 (2018) 134.

2. Z. Zhou, F. Chen, T. Kuang, L. Chang, J. Yang, P. Fan, Z. Zhao and M. Zhong, *Electrochim. Acta,* 274 (2018) 288.
3. G. Li, Y. Li, J. Chen, P. Zhao, D. Li, Y. Dong and L. Zhang, *Electrochim. Acta,* 245 (2017) 941.
4. G. P. Kim, S. Park, I. Nam, J. Park and J. Yi, *J. Power Sources* 237 (2013) 172.
5. C. Kuang, W. Zeng, H. Ye and Y. Li, *Phys. E.,* 97 (2018) 314.
6. M. Arif, A. Sanger, M. Shkir, A. Singh and R.S. Katiyar, *Phys. B.,* 552 (2019) 88.
7. J. Tian, Q. Shao, X. Dong, J. Zheng, D. Pan, X. Zhang, H. Cao, L. Hao, J. Liu, X. Mai and Z. Guo, *Electrochim. Acta,* 261 (2018) 236.
8. N. S. Palani, N. S. Kavitha, K. S. Venkatesh, K. Ashok Kumar, V. Thirumal , A. Pandurangan, C. Sekar and R. Ilangovan, *J. Solid State Electrochem*., 22 (2018) 3273.
9. Y. Tan, Q. Gao, W. Tian, Y. Zhang and J. Xu, *Microporous Mesoporous Mater*., 200 (2014) 92.
10. H. W. Nesbitt, D. Legrand and G. M. Bancroft, *Phys. Chem. Minerals,* 27 (2000) 357.
11. J. Li, X. Qian, Y. Peng and J. Lin, *Mater. Lett*., 224 (2018) 82.
12. K. Ding, B. Wei, Y. Zhang, C. Li, X. Shi and J. Pan, *Int. J. Electrochem. Sci*., 12 (2017) 8381.
13. K. Ding, T. Okajima and T. Ohsaka, *Electrochemistry,* 75 (2007) 35.
14. M. Krajewski, M. Michalska, B. Hamankiewicz, D. Ziolkowska, K.P. Korona, J.B. Jasinski, M. Kaminska, L. Lipinska and A. Czerwinski, *J. Power Sources,* 245 (2014) 764.
15. T.-F. Yi, H. Liu, Y.-R. Zhu, L.-J. Jiang, Y. Xie and R.-S. Zhu, *J. Power Sources,* 215 (2012) 258.